RSC Advances

PAPER

View Article Online
View Journal | View Issue

Cite this: *RSC Adv.*, 2016, **6**, 73045

Electrospray loading and release of hydrophobic gramicidin in polyester microparticles†

Silvana Maione,[ab] Luis J. del Valle,*[ab] Maria M. Pérez-Madrigal,[ab] Carlos Cativiela,[c] Jordi Puiggalí[ab] and Carlos Alemán*[ab]

Received 28th April 2016
Accepted 14th July 2016

DOI: 10.1039/c6ra11056h

www.rsc.org/advances

Gramicidin (GA), a very hydrophobic pentadecapeptide with important biological activities (*i.e.* in addition to its well-known antimicrobial and antibiotic activities, GA has been recently identified as a potent therapeutic agent against different carcinomas), has been loaded by electrospraying in poly(tetramethylene succinate) (PE44), a biodegradable and biocompatible aliphatic polyester. Microspheres (average diameter: 5.0 ± 0.7 μm) were successfully obtained from the mixture of GA and PE44 solutions in ethanol and chloroform, respectively. The loading of the peptide, which has been proved by FTIR and X-ray photoelectron spectroscopies, essentially occurred at the surface of the microspheres, as was reflected by scanning electron microscopy micrographs and atomic force microscopy phase images. In spite of this, the thermal stability of the polyester matrix remained essentially unaltered, even though the wettability decreased. The release of GA in phosphate buffer saline (PBS) was limited by the very low solubility of the peptide in aqueous solution, a fast burst effect followed by the establishment of equilibrium after 5 days of being observed in this hydrophilic environment. The release behaviour was very different when the hydrophilicity of the medium was reduced by adding ethanol. In this case, a very fast but sustained release was identified during the first few hours. On the other hand, biological tests have demonstrated that GA retains its antimicrobial activity after loading and does not alter the biocompatibility of PE44. Our results prove that, despite its hydrophobicity and relatively large number of residues, the loading of GA in a polymeric matrix represents an alternative strategy for the release of this versatile peptide in cancer therapy.

Introduction

Gramicidin (GA) is a linear hydrophobic pentadecapeptide produced by *Bacillus brevis*[1] with the sequence formyl-L-Xxx-Gly-L-Ala-D-Leu-L-Ala-D-Val-L-Val-D-Val-L-Trp-D-Leu-L-Yyy-D-Leu-L-Trp-D-Leu-L-Trp-ethanolamine, where Xxx and Yyy depend on the GA molecule type. For example, commercial samples of GA usually contain types A, B and C, in which Xxx can be either Val or Ile for the three species and Yyy = Trp, Phe and Tyr for type A, B and C, respectively. This unique sequence of alternating L- and D-amino acids renders GA sensitive to the environment.[2–7] More specifically, the pitch, handedness and dimeric configuration of the helix adopted by GA depends on the dielectric constant of its environment.

From a functional point of view, GA is well known because of its ability to kill pathogenic microorganisms. For example, it exhibits activity against Gram-positive bacteria, even though its mechanism of action is not entirely understood.[8–12] GA is also used as antibiotic but its toxicity due to hemolytic characteristics limited that application.[13,14] In the last few years, GA has been proposed as a potential therapeutic agent for different carcinomas.[15–18] Thus, studies *in vivo* revealed that GA effectively reduces the growth of renal cell carcinoma (RCC) cells,[15] which are highly resistant to conventional treatments. The peptide blocks ATP generation by inhibiting oxidative phosphorylation and glycolysis, leading to cellular energy depletion and non-apoptotic cell death. Form these works it was concluded that GA reduced the growth of human RCC xenograft tumors without causing significant toxicity.[16] GA-treated tumors also displayed physiologic and molecular features consistent with the inhibition of hypoxia-inducible factor-dependent angiogenesis. Wijesinghe and co-workers[17] reported that GA channels inserted into the cancer cells open flux of protons into the cytoplasm and disrupt balance of other monovalent cations, which induces cell apoptosis. Rao *et al.*[18] introduced a strategy to kill selectively multi-drug-resistant cells that express the breast cancer resistance protein (BCRP). This approach was based on specific stimulation of ATP hydrolysis by BCRP transporters

[a]*Department of Chemical Engineering, ETSEIB, Universitat Politècnica de Catalunya, Av. Diagonal 647, Barcelona 08028, Spain. E-mail: luis.javier.del.valle@upc.edu; carlos.aleman@upc.edu*

[b]*Center for Research in Nano-Engineering, Universitat Politècnica de Catalunya, Campus Sud, Edifici C', C/Pasqual i Vila s/n, Barcelona 08028, Spain*

[c]*Departamento de Química Orgánica, Instituto de Síntesis Química y Catálisis Homogénea-ISQCH, CSIC-Universidad de Zaragoza, C/Pedro Cerbuna, 12, 50009 Zaragoza, Spain*

† Electronic supplementary information (ESI) available. See DOI: 10.1039/c6ra11056h

with subtoxic doses of curcumin combined with stimulation of ATP hydrolysis by Na^+, K^+-ATPase with subtoxic doses of GA. More biomedical applications of GA have been recently reviewed by Gurnev and Nestorovich,[19] who also summarized the role of channel-forming peptides for cancer therapy.

In spite of its biomedical interest, encapsulation of GA, which represents a major challenge due to the insolubility of this peptide, has been scarcely studied.[20] In a very recent study, Wu and coworkers[20] used graphene oxide (GO) as nanocarrier to load and deliver GA. In spite of the effective antibacterial activity exhibited by GA-loaded GO nanoparticles, other studies[21] evidenced that GO exhibits dose-dependent toxicity to cells and living systems. Accordingly, the use of GO as a biocompatible material was suggested to be controversial when this material is applied for biomedical engineering. On the other hand, solid peptide nanoparticles have been prepared using amino acid sequences related with those of GA.[22,23] Within this context, Dittrich and Meier[22] obtained solid spherical particles with diameters of around 500 nm and low-size polydispersity using a highly hydrophobic peptide decamer made of acetylated L-Lys, L-Trp and D-Leu. Also, Meier and coworkers[23] prepared peptide particles, which were hypothesized to be multicompartment micelles, using an undecamer made of a repetitive L-Trp-D-Leu motif in a hydrophobic block and an N-terminally attached hydrophilic (Lys) section. Nevertheless, the potential biomedical applications of the peptides used to prepare such nano- and micro-structures have not been examined and, indeed, is not expected to be similar to those of parent GA.

In this we report a simple strategy to prepare poly(tetramethylene succinate) (PE44) microspheres loaded with GA by means of the electrospraying technique. After comparison of the chemical, morphological and thermal properties of GA-loaded and unloaded PE44 microspheres (*i.e.* PE44 microspheres without GA), hereafter denoted PE44-GA and U-PE44, respectively, the delivery of the peptide has been examined in two media. Results indicate that the release behaviour is highly dependent on the hydrophilicity of the medium.

Methods

Materials

Poly(tetramethylene succinate) is a commercial product (Bionolle® 1001) supplied by Showa Denko K.K. (Germany). The polymer has a melt flow index of 1.6 g/10 min (measured at 190 °C under a load of 2.16 kg according to ASTM-D1238). GA was purchased from Sigma-Aldrich (G5002), containing 80–85%, 6–7%, 5–14% and <1% of type A, B, C and D, respectively.

Electrospraying

PE44 and GA were dissolved in chloroform and ethanol, respectively, by stirring at 80 rpm overnight. The two solutions were mixed in a resealable glass vial to prepare the electrospray solution, which was homogenized by stirring at 80 rpm for 1 h. The weight percentages of PE44 and GA in the resulting electrospray solution were 2.5 wt% and 0.25 wt% (*i.e.* 10% respect to the polymer weight), respectively. Operational conditions for the preparation of PE44-GA microspheres by electrospraying were optimized, even though results obtained using the selected processing conditions are the only displayed in this work. Electrosprayed PE44-GA microspheres were collected on a target placed at 25 cm from the needle tip (18 G, inside diameter 0.84 mm). A voltage of 30 kV was applied to the target using a high-voltage supply (Gamma High Voltage Research, ES30-5W). Polymer solutions were delivered *via* a KDS100 infusion syringe pump (KD Scientific, USA) to keep the flow rate at 1 mL h^{-1}. All electrospraying experiments were carried out at room temperature. The procedure and the parameters used to prepare blank samples, which consist of U-PE44 microspheres, were identical to those described for PE44-GA with the obvious exception that ethanol did not contain GA.

Characterization

Detailed inspection of texture and morphology of microspheres was conducted by scanning electron microscopy (SEM) using a Focus Ion Beam Zeiss Neon 40 instrument (Carl Zeiss, Germany). Carbon coating was accomplished using a Mitec K950 Sputter Coater fitted with a film thickness monitor *k*150×. Samples were visualized at an accelerating voltage of 5 kV. The diameter of the microspheres was measured with the SmartTiff software from Carl Zeiss SMT Ltd.

Atomic Force Microscopy (AFM) was conducted to obtain topographic and phase images of the surface of microspheres using silicon TAP 150-G probes (Budget Sensors, Bulgaria) with a frequency of 150 kHz and a force constant of 5 N m^{-1}. Images were obtained with an AFM dimension microscope using the NanoScope IV controller under ambient conditions in tapping mode. The row scanning frequency was set between 0.4 and 0.6 Hz. The Root Mean Square roughness (RMS Rq), which is the average height deviation taken from the mean data plane, was determined using the statistical application of the NanoScope Analysis software (1.20, Veeco).

Aggregation phenomena in raw materials (*i.e.* PE44 and GA) were studied by dynamic light scattering (DLS) using the conditions (solvent and concentration) selected for the processing by electrospraying. Measurements were performed using a NanoBrook Omni Zeta Potential Analyzer from Brookhaven Instruments Corporation.

The specific surface area of U-PE44 and PE44-GA was determined by the Brunauer–Emmett–Teller (BET) technique under standard conditions using a Micromeritics Tristar 3000 analyzer and using N_2 as adsorption gas. Prior to the measurement, the sample was outgassed at 40 °C for 240 minutes (~0.15 mbar).

The degree of crystallinity of the PE44 and the electrosprayed microspheres was analyzed by means of Wide-Angle X-ray Diffractometer (WAXD) using the X'Pert Pro System (PANalytical, Netherland). The diffraction patterns were obtained using Cu Kα ($\lambda = 0.1542$ nm) X-ray source operating at 30 kV and 30 mA. Samples were examined using the powder form. The degree of crystallinity (χ_c) was estimated using PeakFit v4.0 software (Jandel Scientific Software, AISN Software Inc.) according to Hindeleh and Johnson's method and the following equation:

$$\chi_c = \frac{A_C}{A_C + A_A} \quad (1)$$

where: A_A and A_C are the calculated area under amorphous and crystalline curves of deconvoluted X-ray pattern, respectively.

Additionally, approximated theoretical curves allow calculating crystalline size using the Scherrer equation:

$$L_{(hkl)} = \frac{K\lambda}{B\cos\theta} \quad (2)$$

where $L_{(hkl)}$ is the average crystallite size in the orthogonal direction to the plane (*hkl*), θ is the Bragg angle, λ is the X-ray wavelength, B is the FWHM of the diffraction peak for the plane (*hkl*) and K is the Scherrer constant ($K = 0.9$ for polymers).

A UV-3600 (Shimadzu) UV-vis/NIR spectrophotometer controlled by the UVProbe V2.31 software was used to record UV-vis spectra of GA at room temperature in the 200–400 nm range, with a bandwidth of 2 mm, a scan speed of 600 nm min^{-1}, and a sampling interval of 1 nm.

FTIR spectroscopy was used to assess the presence of peptide in PE44-GA samples. Absorption spectra were recorded with a Fourier Transform FTIR 4100 Jasco spectrometer in the 4000–600 cm^{-1} range. A Specac model MKII Golden Gate attenuated total reflection (ATR) with a heated Diamond ATR Top-Plate was used. FTIR spectroscopy was also used to examine the secondary structure of GA in prepared PE44-GA microspheres. This information was derived from the peaks in the amide I and amide II regions, which were deconvoluted and fitted to Gaussian functions using the PeakFit 4 (Jandel Scientific Software, AISN Software Inc.) and OriginPro 8 software, respectively.

Circular dichroism (CD) measurements were carried out in a Jasco J-810 spectropolarimeter at 22 °C using a quartz cuvette. The CD data were recorded with standard sensitivity (100 mdeg), in the 150–260 nm range, with bandwidth of 2 mm, response time of 0.5 s and scanning speed of 500 nm min^{-1}. The reported spectra correspond to the average of five scans, the raw spectra being smoothed by the Savitzky–Golay algorithm and deconvolutioned for analysis and interpretation.

X-ray photoelectron spectroscopy (XPS) analyses were performed in a SPECS system equipped with a high-intensity twin-anode X-ray source XR50 of Mg/Al (1253 eV/1487 eV) operating at 150 W, placed perpendicular to the analyzer axis, and using a Phoibos 150 MCD-9 XP detector. The X-ray spot size was 650 mm. The pass energy was set to 25 and 0.1 eV for the survey and the narrow scans, respectively. Charge compensation was achieved with a combination of electron and argon ion flood guns. The energy and emission currents of the electrons were 4 eV and 0.35 mA, respectively. For the argon gun, the energy and the emission currents were 0 eV and 0.1 mA, respectively. The spectra were recorded with a pass energy of 25 eV in 0.1 eV steps at a pressure below 6×10^{-9} mbar. These standard conditions of charge compensation resulted in a negative but perfectly uniform static charge. The C1s peak was used as an internal reference with a binding energy of 284.8 eV. High-resolution XPS spectra were acquired by Gaussian/Lorentzian curve fitting after S-shape background subtraction. The surface composition was determined using the manufacturer's sensitivity factors.

Thermal degradation was studied at a heating rate of 20 °C min^{-1} (sample weight *ca.* 5 mg) with a Q50 thermogravimetric analyser of TA Instruments and under a flow of dry nitrogen. Test temperatures ranged from 30 to 600 °C.

Contact angle measurements were obtained using the sessile water drop method at room temperature and controlled humidity. Images of 0.5 μL distillated water drops on surfaces collecting the microspheres were recorded after stabilization (10 s) with the equipment OCA 20 (DataPhysics Instruments GmbH, Filderstadt). The software SCA20 was used to analyze the images and acquire the contact angle value. Contact angle values were obtained as the average of 15 independent measures for each sample.

GA-release experiments

Mats with GA-loaded microspheres were cut into small squares (2×2 cm^2 and around 15–20 mg of weight) which were weighed and placed into polypropylene tubes. Phosphate buffer saline (PBS, pH 7.4) and PBS supplemented with 70 v/v% of ethanol (PBS–EtOH) were considered as release media. The addition of ethanol to hydrophilic PBS increases the hydrophobicity of the medium and provokes some swelling effect, both favoring the release of hydrophobic drugs as GA.[24] The released GA was quantified using the Bradford reagent. Assays were carried out by immersing sample mats in 30 mL of the release medium at 37 °C for 1 week. Aliquots (1 mL) were drawn from the release medium at predetermined intervals, and an equal volume of fresh medium was added to the release vessel. The Bradford reaction was performed in microtiter plate mode and the absorbance measurement in a reader plate. Calibration curves were obtained by plotting the absorbance measured at 595 nm against drug concentration. Finally, the mats were dissolved in chloroform and the residual drug was extracted in ethanol for quantification. All tests were performed in triplicate to control the homogeneity of the release, and the results were averaged.

Antimicrobial test: inhibition of bacterial growth

Escherichia coli (*E. coli*) and *Staphylococcus aureus* (*S. aureus*) were selected to evaluate the activity of loaded GA against bacteria. The bacteria were previously grown aerobically by exponential phase in Luria–Bertani (LB) broth (at 37 °C and agitated at 80 rpm). In addition to PE44-GA samples, U-PE44 (negative control) and gentamicin discs (positive control), an antibiotic used to treat many types of bacterial infections, were also considered for antimicrobial assays.

The agar diffusion test was performed in Petri dishes of 90 mm. A standardized 0.5 McFarland of the test strain culture was inoculated homogeneously on the surface of LB agar using a sterile nylon swab. Then, samples were pasted onto the agar plate. Bacteria were incubated at 37 °C for 24 hours and the inhibition zone for each sample on the plate was observed.

Cytotoxicity and cell adhesion

Madin Darby Canine Kidney (MDCK) cells were cultured in DMEM high glucose supplemented with 10% FBS, penicillin (100 units per mL), and streptomycin (100 μg mL^{-1}). The cultures were maintained in a humidified incubator with an atmosphere of 5% CO_2 and 95% O_2 at 37 °C. Culture media were changed every two days. When the cells reached 80–90% confluence, they were detached using 1–2 mL of trypsin (0.25% trypsin/EDTA) for 5 min at 37 °C. Finally, cells were re-suspended in 5 mL of fresh medium, their concentration being determined by counting in a Neubauer camera using 0.4% trypan blue as a dye vital.

U-PE44 and PE44-GA samples were placed in plates of 24 wells and sterilized using UV-light for 15 min in a laminar flux cabinet. Controls were simultaneously performed by culturing cells on the surface of the tissue culture polystyrene (TCPS) plates. For adhesion assays, an aliquot of 50 μL containing 5×10^4 cells was deposited onto each sample. Then, cell attachment was promoted by incubating under culture conditions for 30 min. Finally, 500 μL of the culture medium were added to each well. After 24 h, non-attached cells were washed out, while attached cells were quantified. Cytotoxicity was also determined after 24 h of culture. All viability measures were relative to TCPS used as control (*i.e.* 100%).

Viability for cytotoxicity and cellular adhesion were evaluated by the colorimetric MTT assay. This assay measures the ability of the mitochondrial dehydrogenase enzyme of viable cells to cleave the tetrazolium rings of the MTT and form formazan crystals, which are impermeable to cell membranes and, therefore, are accumulated in healthy cells. This process is detected by a colour change: the characteristic pale yellow of MTT transforms into the dark-blue of formazan crystals. Specifically, 50 μL of MTT solution (5 mg mL^{-1} in PBS) were added to each well. After 3 h of incubation, samples were washed twice with PBS and stored in clean wells. In order to dissolve formazan crystals, 200 μL of DMSO/methanol/water (70/20/10% v/v) was added. Finally, the absorbance at 570 nm was measured using a microplate reader (Biochrom EZ Read 400, Biochrom). The resulting viability results were normalized to TCPS control as relative percentages. Results were derived from the average of six replicates ($n = 6$) for each independent experiment. ANOVA and Tukey tests were performed to determine statistical significance, which was considered at a confidence level of 95% ($p < 0.05$).

Results and discussion

PE44 has been reported to be perfectly soluble in chloroform, this solvent being previously used to process different nano- and microstructures with the same polyester.[25,26] Although hydrophobic GA is hardly soluble in water and tends to form colloidal suspensions in this solvent, it is soluble in a number of organic solvents including those used in the electrospray solution. Initially, the impact of different solvents on the stability of GA was examined by absorption spectroscopy. Although the UV-vis spectrum of GA is not characteristic of its entire structure,[27] uncharacteristic absorbance at 200–300 nm should be clearly detected due to the chromophoric units of the molecule (*i.e.* the four Trp of GA of type A, which is the most abundant in the purchased sample).[28–30] Results, which are displayed in Fig. S1,† indicated that the spectrum of GA remains practically unaltered when the ethanol solvent is replaced by methanol, chloroform, acetonitrile, formic acid and dichloromethane while important changes occur in water. Thus, the absorption peaks at around 280 and 288 nm observed for organic solvents become a shoulder in water (*i.e.* complete description of the UV-vis spectra is provided in the ESI†). In addition, the solubility of the peptide in aqueous solution was observed to be very low in comparison to the other solvents. These results are fully consistent with DLS measures for GA in water, ethanol and chloroform (Fig. 1). As it can be seen, the lowest and highest effective particle diameter (D_{eff}) was obtained in ethanol ($D_{eff} =$ 1.6 μm) and water ($D_{eff} = 10.1$ μm), respectively, while the size of the aggregates in chloroform ($D_{eff} = 3.5$ μm) was similar to that in ethanol. According to these results, the electrospray solution described in the Methods section, which was obtained by mixing PE44 and GA solutions in chloroform and ethanol, respectively, was appropriated for loading the peptide.

Once the solvents were selected, operational parameters (*i.e.* applied voltage, tip–collector distance and flow rate) and solution properties (*i.e.* viscosity, surface-tension, volatility and concentration) were optimized to obtain regular microparticles of well-defined diameter. In general, the charge density on the droplet increases with the voltage, favouring the breakup of the liquid jet when the polymer concentration is low. However, high voltages promote the formation of microparticles with a broad distribution of sizes since multi-jets become irregular. The particle diameter increases with the distance between the tip and the collector because breakup becomes insufficient. The flow rate, which affects the charge density, is typically used to control the sphericity (*i.e.* high flow rates are characteristic of a poor sphericity). Solution properties also affect the fission of droplets, which is hampered when the surface tension is too high. Solution viscosity, which depends on the solvent, temperature and, especially, the polymer concentration and

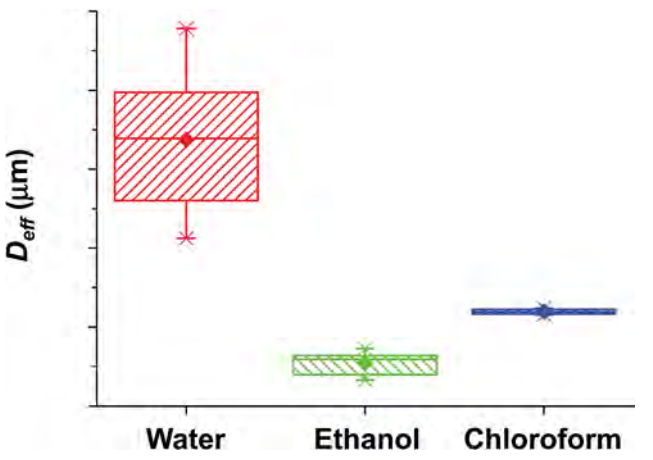

Fig. 1 Effective diameter (D_{eff}, in μm) as measured by DLS of GA aggregates in different solvents.

molecular weight, affects both the size and shape of the particles. Thus, breakup and deformation are hampered when the viscosity is high, fibres or particles being obtained from high or low viscosity solutions, respectively. These criteria were used to optimize the electrospraying conditions used in this work, which are summarized in the Methods section.

SEM micrographs of U-PE44 and PE44-GA electrosprayed particles are compared in Fig. 2. In both cases microspheres were abundant and present some irregularities, which have been attributed to different degrees of collapse provoked by the low PE44 concentration (*i.e.* 2.5 wt%). In spite of these similarities, the peptide induces some important differences between the loaded and unloaded microspheres. Thus, U-PE44 particles present a wrinkled surface with well-defined folds homogeneously distributed onto it. These folds are placed at higher levels than the core of the particle, resulting in a homogeneous distribution of small cavities at the surface. In contrast, the cavities defined by the folds are filled in PE44-GA samples, indicating that peptide is loaded at the surface. This feature was corroborated by the AFM images displayed in Fig. 3. Thus, comparison between phase and height images recorded for U-PE44 and PE44-GA samples clearly indicate that GA particles are located on the surface of the microspheres. The diameter of GA particles, which was estimated by analysing the cross-sectional profiles displayed in Fig. S2,† varied between 50 nm and 114 nm. AFM images also evidenced that the RMS Rq was slightly higher for U-PE44 than for PE44-GA.

It was not possible to have straightforward evidences of the morphology at the interior of the microspheres. Unfortunately, application of FIB-SEM led to the melting of the microparticles, while the application of alternative methodologies, like the one proposed by Wang *et al.*[31] and Zhang *et al.*,[32] was not feasible because it requires the sample to be dissolved in water (*i.e.* both U-PE44 and PE44-GA microspheres tend to aggregate when interacting in aqueous solutions). However, the preparation process and the surface morphology of samples displayed in Fig. 2 is similar to that of electrosprayed aluminum microspheres,[33] which were found to be denser in the surface region than in the interior. This phenomenon, which should be attributed to the electrospraying process, is presumable due to the fact that aggregates on the surface have more opportunity to move and re-arranged relative to the interior aggregates.

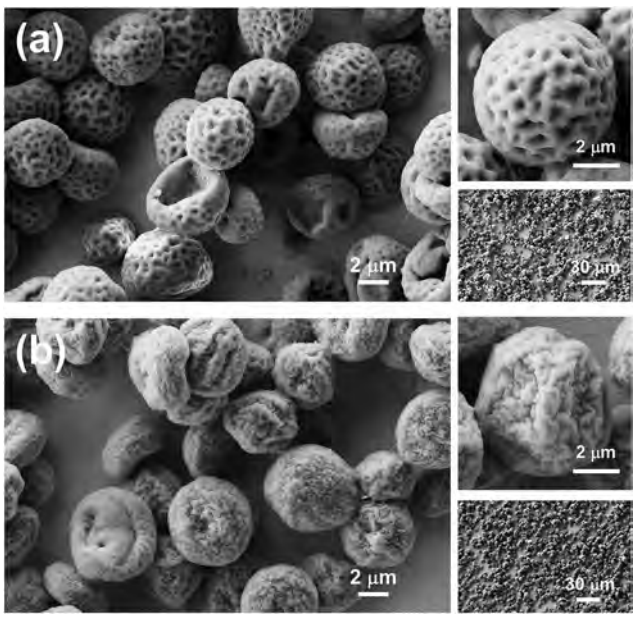

Fig. 2 High and low magnification SEM micrographs of (a) U-PE44 (blank sample) and (b) PE44-GA electrosprayed microspheres.

The generation of electrosprayed particles is widely accepted to be controlled by two main mechanisms: solvent evaporation from droplets *en route* from the tip to the collector, and contemporaneous polymer diffusion during evaporation.[34] Rapid polymer diffusion does not necessarily lead to spherical particles but will ensure solid, dense particles. Both these mechanisms are dictated by the characteristics of the electrosprayed polymer solution itself, which in turn depend on the molecular weight and polymer concentration. Theoretically, the GA should be distributed evenly throughout the electrosprayed PE44 microparticles, however, it was scattered throughout the microparticles in various sizes (*i.e.* from 50 nm to 114 nm). This distribution pattern is closely related to the structure and stability of water-in-oil emulsions.[35,36] The polar phase composed of GA dissolved in ethanol was dispersed into the organic phase, composed of PE44 dissolved in chloroform during the own electrospraying process. As a consequence, the drug was close to the surface the microparticles.

Although the average particle diameter (d) was very similar for both U-PE44 and PE44-GA (5.1 ± 0.5 μm and 5.0 ± 0.7 μm, respectively), addition of 0.25 wt% GA to the electrospray solution slightly affects the diameter distribution (Fig. 4). Thus, a narrow distribution with kurtosis of 1.34 at a confidence interval (CI) of 95% in the range 4.9–5.2 μm is observed for U-PE44, while PE44-GA shows a broader distribution with kurtosis of 0.04 in the CI of 95% (4.9–5.2 μm). As the electrospray operational conditions were identical for both systems, the movement of the diameter distribution of PE44-GA towards higher values supports that the peptide is loaded in the microspheres and particularly at their surface. Processing has a notable effect on the dimensions of polymer particles. Thus, the d value determined for U-PE44 electrosprayed microparticles is 20% higher than the effective diameter determined by DLS ($D_{eff} = 4.1 \pm 0.6$ μm) for the raw material (*i.e.* PE44 powder coming from synthesis). The surface area of the electrosprayed particles, which is relevant for the diffusion of the GA molecules from particle to solvent, was determined by BET. This area increased from 2.5705 $m^2\ g^{-1} \pm 0.0513\ m^2\ g^{-1}$ for U-PE44 to 6.1361 $m^2\ g^{-1} \pm 0.2548\ m^2\ g^{-1}$ for PE44-GA, indicating that diffusion phenomena should be favoured in latter with respect to the former.

Fig. S3† compares the WAXD patterns registered for U-PE44 and PE44-GA microspheres, respectively. Detailed discussion of the X-ray diffractograms, which reflects the PE44 monoclinic crystal lattice,[37] is provided in the ESI.† Deconvolution of the X-ray diffraction patterns into the crystalline peaks and the amorphous halo reveals significant differences between electrosprayed microspheres and the raw-materials (Table S1†). As

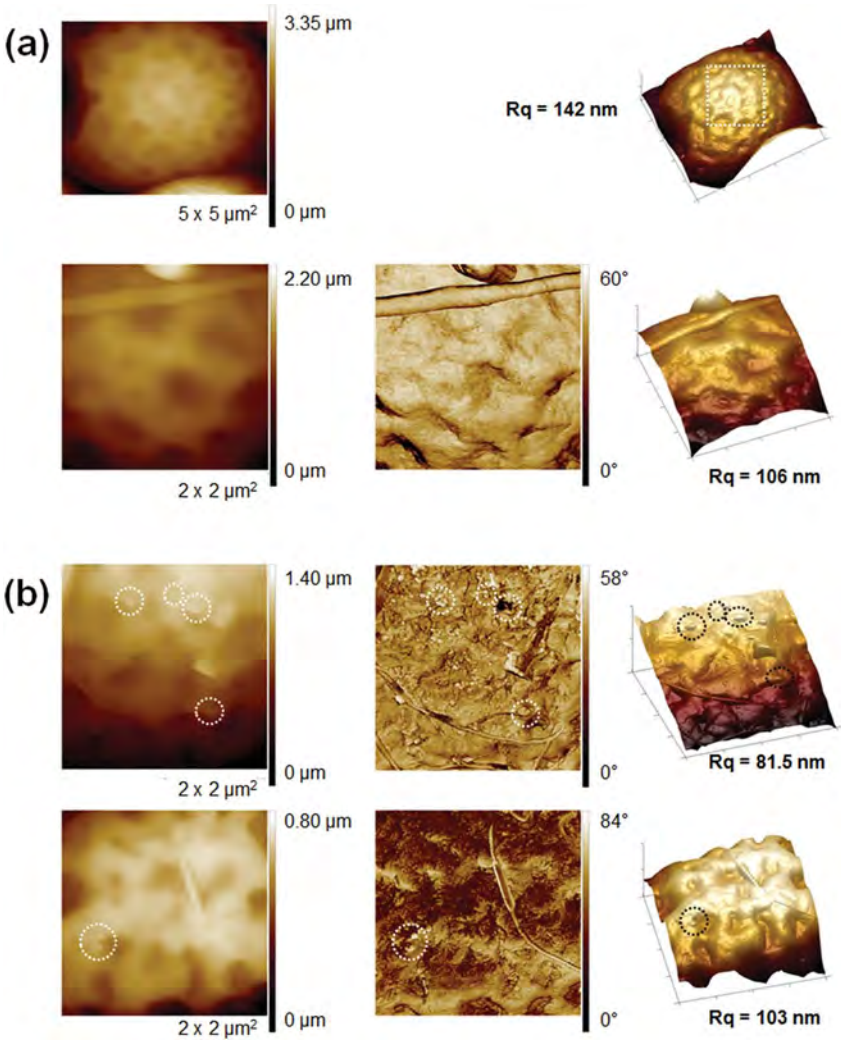

Fig. 3 AFM images of (a) U-PE44 (blank sample) and (b) PE44-GA electrosprayed microspheres: 2D height images (left column), 2D phase images (middle column), and 3D height images (right column). Pointed circles in images displayed in (b) indicate GA aggregates (cross-section profiles of these particles are shown in Fig. S1†).

it can be seen, the crystallinity of the electrosprayed microparticles increases significantly upon the loading of GA ($\chi_c = 0.42$ and 0.76 for U-PE44 and PE44-GA). Indeed, PE44-GA is more crystalline than the reference sample ($\chi_c = 0.63$), even though the origin of their crystallinities are different. The sample prepared by solvent-casting allows a slow settlement of the polymer chains, resulting in a χ_c value higher than that of U-PE44. In contrast, for PE44-GA the increment in the χ_c value with respect to U-PE44 must be attributed to the contribution of the crystalline GA.

Comparison of the FTIR spectra of U-PE44 and PE44-GA samples corroborates the loading of the peptide during the electrospraying process (Fig. 5). Thus, the amide I band, which is governed by the stretching vibrations of the C=O and C–N groups, and the amide II band, which arises from the coupling between the N–H in-plane bending and the C–N stretching modes, are recognizable at approximately 1629 and 1535 cm^{-1}, respectively, for PE44-GA. These two amide bands are clearly distinguishable from the C=O stretching of aliphatic esters that appears as an intense and sharp band at 1712 cm^{-1} for both U-PE44 and PE44-GA.

Analysis of the FTIR amide I and amide II regions has been used to determine the structural characteristics of GA loaded into PE44 microspheres. Results, which are displayed in Fig. S4† for unloaded and loaded GA, indicate that the amide I band correspond to the β-helix conformation. The component at 1632 cm^{-1} is present in the two samples and has been related with the $\beta^{6.3}$-helix.[38] The component at 1650 cm^{-1}, which corresponds to the $\beta^{5.6}$-helix,[38] is clearly recognizable for the loaded peptide while it is only a shoulder in the spectrum of unloaded GA. These results suggest that two different β-helices coexist in PE44-GA while the $\beta^{6.3}$-helix is clearly the predominant for the GA in solution. The latter has been corroborated by comparing the CD spectrum acquired for GA dissolved in ethanol (Fig. S5†) with those reported in the literature.[7] The influence of the PE44 matrix in the peptide conformation is also supported by relative intensity changes in the four components of the FTIR amide II band (Fig. S4†).

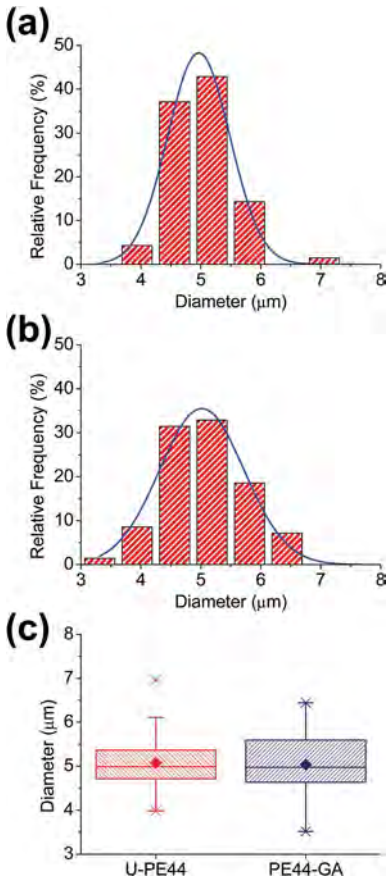

Fig. 4 Diameter distribution of electrosprayed (a) U-PE44 and (b) PE44-GA microparticles. (c) Comparison of the diameters using a box-chart representation. The box range is determined by the 25th and 75th percentiles. The whiskers (×) are determined by the 1st and 99th percentiles. The (–) are the maximum and minimum values, (◆) corresponds to the mean, and the horizontal line into box is the median.

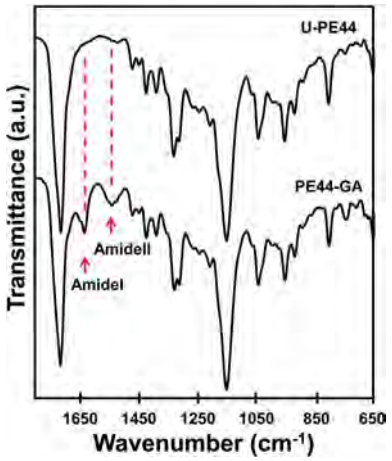

Fig. 5 FTIR spectra of electrosprayed U-PE44 and PE44-GA microparticles in the range 1850–1000 cm^{-1}.

The chemical structure of U-PE44 and PE44-GA particles was further characterized by XPS, compositions being compared in Table 1. The penetration of X-ray radiation using the conditions

Table 1 Atomic percent composition (C1s, N1s and O1s) obtained by XPS for U-PE44 and PE44-GA samples

Sample	C1s	N1s	O1s
U-PE44	69.23	0.26	30.51
PE44-GA	68.09	4.57	27.34

described in Methods section is expected to be ~10 nm, even though in this case the penetration is unknown because of both the porosity (Fig. 2a) of U-PE44 microspheres. In any case, radiation reaches the surface of the metallic substrate (aluminum foil) used as collector, which is only partially covered by electrosprayed microspheres. This feature explains the detection of a small percentage of nitrogen in U-PE44 samples, which has been attributed to the aluminum foil substrate. It should be noted that we also detected nitrogen in the atomic composition of polymeric microstructures deposited onto metallic substrates, even though in those cases the substrate was stainless steel.[39] However, the N1s increases from 0.26% in U-PE44 to 4.57% in PE44-GA, supporting the successful incorporation of the peptide. For U-PE44 the C/O ratio, 2.27, is close to the theoretical value of 2.00, while such ratio increases to 2.49 for PE44-GA. Although the increment of the C/O ratio in the latter has been associated to the loading of peptide, it is important to point out that the experimental values of C/O ratio are influenced by the presence of hydrocarbon contamination. This is commonly present in samples subjected to XPS analysis and can be traced back to typical laboratory environment and the pumping system.[40]

High-resolution XPS spectra in the C1s and O1s regions are displayed in Fig. 6. Deconvolution of the C1s peak led to three and four Gaussian curves for U-PE44 and PE44-GA, respectively. Three of such curves have been attributed to saturated C–C/C–H (284.2 eV), C–O (286.1 eV) and C═O (288.7 eV) bonds of PE44 chains,[41,42] while the fourth curve of PE44-GA corresponds to the (O═)C–NH peptide bonds (287.3 eV).[43,44] The O1s signal

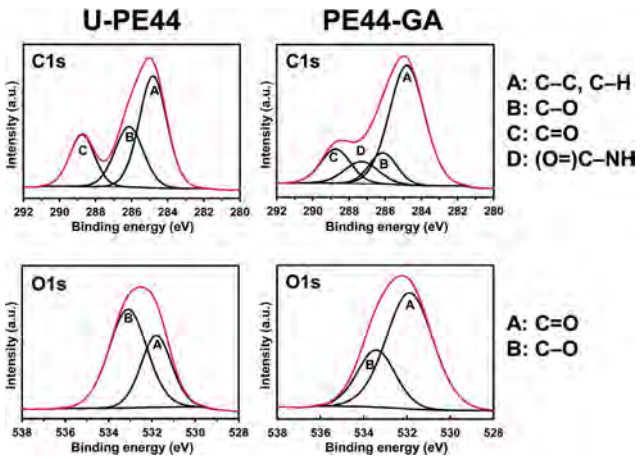

Fig. 6 High-resolution XPS spectra for U-PE44 and PE44-PGA: C1s and O1s regions. The red line corresponds to the experimental profile while the black lines are the peaks from deconvolution. The bonds associated to the deconvoluted peaks are also displayed.

consists of two components, which has been assigned to the C=O (531.87 eV) and C–O bonds (533.42).[39–44] For U-PE44, the C=O component is less intense than the C–O one while the opposite relative intensity order is obtained for PE44-GA due to the incorporation of peptide molecules.

Thermal degradation kinetics of PE44 was studied by Chrissafis *et al.*,[45] a two-step decomposition process being reported. The first one was very small and could only be slightly distinguishable in DTGA thermograms. n^{th}-Order mechanisms were postulated as typical for degradation of polyesters.[46] Specifically $n = 0.75$ and 0.68 and activation energies of 128 and 189 k mol^{-1} were determined for the first and second decomposition steps of PE44, respectively. U-PE44 has a high thermal stability, being the onset degradation temperature higher than 300 °C and, obviously, higher than its melting temperature (115 °C). Incorporation of drugs may affect the thermal stability of the base polymer, a feature that has been considered due to the lower stability of GA (Fig. 7). Thus, the temperature of the main DTGA peak for GA decreases by approximately 50 °C with respect to PE44. In spite of this, minimum changes were detected between U-PE44 and PE44-GA samples (Fig. 7). Thus, the second degradation step seems to proceed slightly faster in such a way that the two stages of degradation are practically not differentiated on the corresponding DTGA curve. In addition, the char yield of PE44-GA slightly increased with respect U-PE44, which is in agreement with the significant residue produced in the decomposition of GA as consequence of its aromatic content.

The water contact angle value determined for U-PE44 is 104° ± 3° (Fig. 8) evidencing the hydrophobic nature of the polymeric matrix. The incorporation of GA enhances the hydrophobicity of the polymeric matrix, the contact angle increasing to 129° ± 2° for PE44-PGA. This is a very attractive result for peptide-release based applications since the low wettability of PE44-GA microspheres in water solvents is expected to be accompanied by a relatively slow delivery in polar environments like PBS.

GA release from electrosprayed microparticles in a given medium is expected to depend on the intermolecular interactions between the peptide and the PE44 matrix. Quantitative release studies were performed considering PE44 microspheres loaded with GA. Both PBS and PBS–EtOH were used as release media. It should be noted that the physical characteristics in a place of the body (*e.g.* pH and hydrophilicity/hydrophobicity ratio) depends on the location. Therefore, comparison of the release rate in PBS and PBS–EtOH is a standard assay to ascertain how changes in the environment affect the drug release. According to previous studies,[24,25] the ethanol supplement facilitates the delivery of highly hydrophobic molecules, such as GA, precluding the establishment of early equilibrium conditions that limit their release in PE44.

Fig. 9 shows the release profile in PBS and PBS–EtOH for GA loaded in PE44 microparticles. The cumulative release plot in PBS for PE44 microspheres loaded with GA exhibits a massive initial burst release up to a maximum percentage (~87%) and a subsequent decrease of the release percentage until a constant value (~70%). The plateau region observed after 5 days is

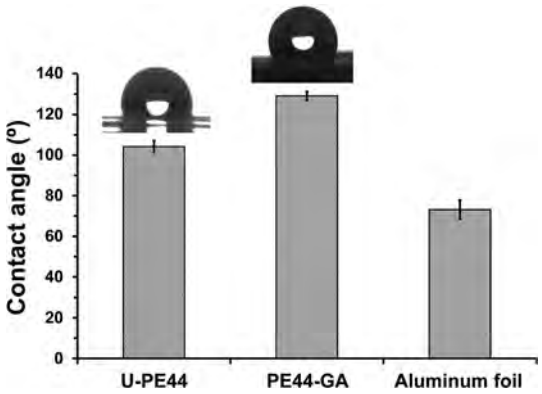

Fig. 8 Contact angle values of U-PE44 and PE44-GA. The contact angle of the aluminum foil used to collect the microspheres is also displayed.

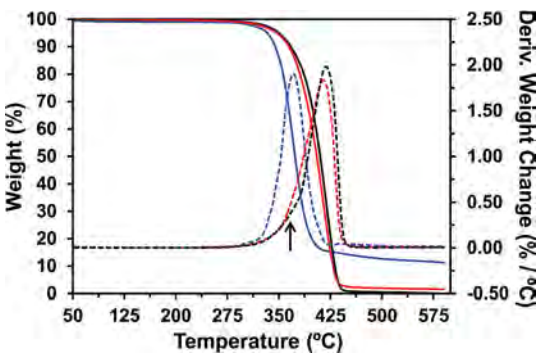

Fig. 7 TGA (solid lines) and DTGA (dashed lines) curves for U-PE44 (black), GA (blue) and the PE44-GA (red). Arrow points out the first degradation step of PE44.

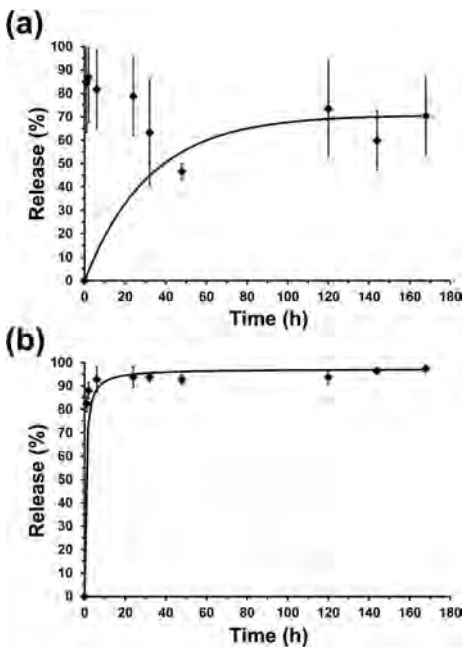

Fig. 9 Release curves in (a) PBS and (b) PBS–EtOH media of GA from PE44-GA microspheres.

consistent with the achievement of that equilibrium value. This behaviour suggests that a small amount of the initially delivered peptide was able to enter again inside the PE44 microparticles to meet the equilibrium condition. It should be remarked that the burst release, which is due to the rapid diffusion of PBS into the microparticles surface, is consistent with the location of the GA near the surface,[47] as was evidenced by AFM and SEM. Also, it should be mentioned that measures about the release of GA in PBS exhibited very poor statistical precision (Fig. 9a), which has been attributed to the poor interaction between GA and water discussed above (Fig. S1† and 1).

The rate of GA release from PE44 microspheres is higher in PBS–EtOH than in PBS, which is consistent with hydrophobic sequence of the peptide. Thus, results displayed in Fig. 9b indicate that, initially, the release of GA was very fast, reaching 92% and 98% of the loaded peptide after 6 hours and 7 days of exposure in PBS–EtOH, respectively. The delivery process in PBS–EtOH is explained by the diffusion of the peptide through the polymeric matrix, which is facilitated by the solvent-induced swelling of PE44 and the weak interactions and the polymeric matrix and peptide.

The loading efficiency (LE) was calculated on the basis of the following formula:

$$\%\ \mathrm{LE} = \frac{[\mathrm{GA}]_{\mathrm{final}}}{[\mathrm{GA}]_{\mathrm{initial}}} \times 100 \qquad (3)$$

where $[GA]_{final}$ is the sum of GA released in PBS–EtOH along 168 h and the GA remaining at the PE44 matrix after such time, and $[GA]_{initial}$ corresponds to the GA concentration in the electrospraying solution related to the content of polymer (w/w%). Results indicated that the average LE for this pentadecapeptide is 41% ± 10% (*i.e.* the LE determined for four replicas varied between 32% and 51%). Although very high drug loading efficiencies (up to ~90%) have been reported for microspheres obtained using electrospraying,[48–50] it should be emphasized that the loading of GA in polymeric matrix is a major challenge due to its insolubility. According to such circumstance, the LE reached in this work, which to the best of our knowledge is the greatest reached for GA (*i.e.* Dittrich and Meier[22] obtained LEs lower than 30%), should be considered relatively high. The LE obtained in the current work should be attributed not only to the electrospraying process but also to the appropriate choice of the polymeric matrix. More specifically, the charge distributions of the peptide and the PE44 matrix exhibit important similarities. Thus, the peptide and ester bonds are the only polar groups in the GA and PE44, respectively, while the charge in the rest of the molecular fragments is homogeneously low, which provides a high hydrophobic character. These similar trends facilitate the formation of stable mixtures that are subsequently used as electrospraying solutions.

The antibacterial activity of PE44 microspheres loaded with GA was tested against *E. coli* and *S. aureus* (as representative of Gram-positive and Gram-negative bacteria, respectively). Results from antimicrobial tests are displayed in Fig. 10. An inhibition zone around both PE44-GA and gentamicin samples is clearly identified for the two tested bacteria indicating that compounds with bactericidal activity diffuse outward from the

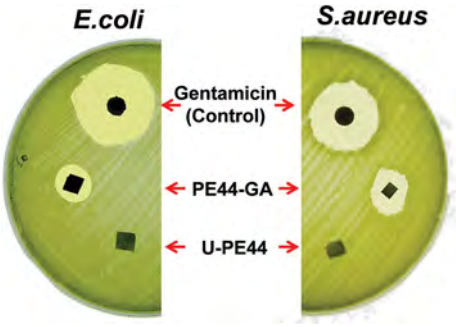

Fig. 10 *E. coli* and *S. aureus* bacterial cultures showing the inhibition zones around PE44-GA and gentamicin (positive control) samples. U-PE44 was also tested as negative control.

samples. Thus, such clear zones are halos of inhibition that indicate the extent of the test organism's inability to survive in the presence of the gentamicin antibiotic and the GA released from the PE44 matrix. Obviously, the area of the clear zone is higher for gentamicin than for PE44-GA since the bacterial growth inhibition promoted by GA depends on the release rate from the polymeric matrix. On the other hand, no inhibition zone has been detected for PE44 samples indicating that, as it was expected, the polymeric matrix is harmless to bacteria.

The response of PE44-GA towards cells was compared with that of U-PE44. Cytotoxicity and cellular adhesion assays were performed considering MDCK epithelial cells. These carcinogenic cells were selected due to their fast growth. Quantitative results are displayed in Fig. 11, TCPS being used as control substrates. As it can be seen, the reduction in the number of viable cells after 24 h of culture was similar for the U-PE44, PE44-GA and the control (Fig. 11a). Similarly, the number of adhered cells by area of material was the same for the three species (Fig. 11b). These results clearly indicate that the incorporation of GA does not alter the biocompatibility of the PE44 matrix, which is practically identical to that of TCPS.

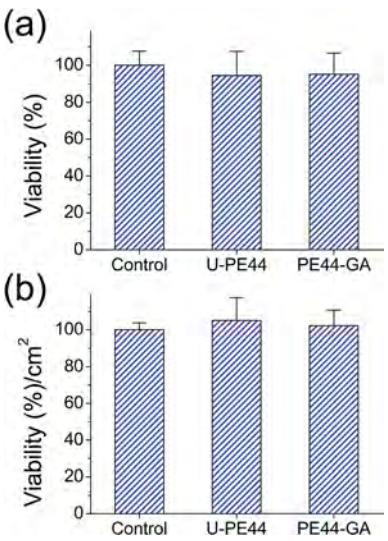

Fig. 11 Viability of MDCK cells in presence of (a) U-PE44 and PE44-GA samples and (b) adhesion cellular onto the microsphere matrices.

Conclusions

The results reported above demonstrate that electrosprayed PE44 microspheres can be used to load GA, a highly hydrophobic pentadecapeptide that has been recently proposed as a potent therapeutic agent against different carcinomas. The loading efficiency is relatively high (41%), which has been attributed to the hydrophobic similarity between the GA and PE44 matrix resulting in a stable combination. The peptide, which is mainly loaded at the surface of the microparticles, enhances the hydrophobicity of the microparticles while the thermal stability remains practically unaltered. After seven days, the delivery in PBS and PBS–EtOH is 70% and 98%, respectively. Thus, the release rate of GA from PE44 microparticles is higher in PBS–EtOH than in PBS due to the remarkably hydrophobicity of this peptide. On the other hand, although FTIR studies suggest that GA undergoes some structural changes upon loading into PE44 microspheres, both the antibacterial activity of the peptide and the biocompatibility of the polymeric matrix are clearly maintained.

In summary, the delivery of therapeutic molecules is tantamount to the success of many medical treatments. With the development of new and superior medical treatment for many diseases, as for example cancer, there is a concomitant demand to encapsulate and release bioactive molecules in a safe, effective and reproducible manner. In this work we have proved that encapsulation and release of GA, a versatile bioactive molecule because of its multiple and varied therapeutic uses, is feasible despite its molecular size and very high hydrophobicity.

Acknowledgements

Authors thank supports from MINECO and FEDER (MAT2015-69367-R, MAT2015-69547-R and CTQ2013-40855-R) and Gobierno de Aragón – Fondo Social Europeo (research group E40). Support for the research of C.A. was received through the prize "ICREA Academia" for excellence in research funded by the Generalitat de Catalunya.

References

1 D. A. Kelkar and A. Chattopadhyay, *Biochim. Biophys. Acta, Biomembr.*, 2007, **1768**, 2011.
2 R. D. Hotchkiss and R. Dubos, *J. Biol. Chem.*, 1940, **132**, 791.
3 F. O'Boyle and B. A. Wallace, *Protein Pept. Lett.*, 2003, **10**, 9.
4 D. A. Doyle and B. A. Wallace, *J. Mol. Biol.*, 1997, **266**, 963.
5 F. Heitz, A. Heitz and Y. Trudelle, *Biophys. Chem.*, 1986, **24**, 149.
6 N. Mobashery, C. Nielsen and O. S. Andersen, *FEBS Lett.*, 1997, **412**, 15.
7 J. A. Killian, K. U. Prasad, D. Hains and D. W. Urry, *Biochemistry*, 1988, **27**, 4848.
8 G. N. Moll, V. van den Eertwegh, H. Tournois, B. Roelofsen, J. A. F. Op den Kamp and L. L. M. van Deenen, *Biochim. Biophys. Acta*, 1991, **1062**, 206.
9 C. Gumila, M.-L. Ancelin, A.-M. Delort, G. Jeminet and H. J. Vial, *Antimicrob. Agents Chemother.*, 1997, **41**, 523.
10 J. W. Liou, Y. J. Hung, C. H. Yang and Y. C. Chen, *PLoS One*, 2015, **10**, e0117065.
11 J. F. Yala, P. Thebault, A. Hequet, V. Humblot, C. M. Pradier and J. M. Berjeaud, *Appl. Microbiol. Biotechnol.*, 2011, **89**, 623.
12 S. Sek, T. Laredo, J. R. Dutcher and J. Lopkowski, *J. Am. Chem. Soc.*, 2009, **131**, 6439.
13 F. Wang, L. H. Qin, C. J. Pace, P. Wong, R. Malonis and J. M. Gao, *ChemBioChem*, 2012, **13**, 51.
14 J. D. Freedman, T. S. Novak, J. D. Bisognano and P. R. Pratap, *J. Gen. Physiol.*, 1994, **104**, 961.
15 J. M. David, T. A. Owens, S. P. Barwe and A. K. Rajasekaran, *Mol. Cancer Ther.*, 2013, **12**, 2296.
16 J. M. David, T. A. Owens, L. J. Inge, R. M. Bremmer and A. K. Rajasekaran, *Mol. Cancer Ther.*, 2014, **13**, 788.
17 D. Wijesinghe, M. C. Arachchige, A. Lu, Y. K. Reshetnyak and O. A. Andreev, *Sci. Rep.*, 2013, **3**, 3650.
18 D. K. Rao, H. Y. Liu, S. V. Ambudkar and M. Mayer, *J. Biol. Chem.*, 2014, **289**, 31397.
19 P. A. Gurnev and E. M. Nestorovich, *Toxins*, 2014, **6**, 2483.
20 H. N. Abdelhamid, M. S. Khan and H.-F. Wu, *RSC Adv.*, 2014, **4**, 50035.
21 K. Wang, J. Ruan, H. Song, J. Zhang, Y. Wo, S. Guo and D. Cui, *Nanoscale Res. Lett.*, 2011, **6**, 8.
22 C. Dittrich and W. Meier, *Macromol. Biosci.*, 2010, **10**, 1406.
23 T. B. Schuster, D. de Bruyn Outboter, E. Bordignon, G. Jeschke and W. Meier, *Soft Matter*, 2010, **6**, 5596.
24 L. J. del Valle, R. Camps, A. Díaz, L. Franco, A. Rodríguez-Galán and J. Puiggalí, *J. Polym. Res.*, 2011, **18**, 1903.
25 S. Murase, M. Aymat, A. Calvet, L. J. del Valle and J. Puiggalí, *Eur. Polym. J.*, 2015, **71**, 196.
26 M. M. Pérez-Madrigal, E. Armelin, L. J. del Valle, F. Estrany and C. Alemán, *Polym. Chem.*, 2012, **3**, 979–991.
27 A. Aszalos, in *Modern Analysis of Antibiotics*, Marcel Dekker Inc, New York, 1986, pp. 32–33.
28 J. Catalán, *Phys. Chem. Chem. Phys.*, 2016, **18**, 15170.
29 D. M. Rogers, N. A. Besley, P. O'Shea and J. D. Hirst, *J. Phys. Chem. B*, 2005, **109**, 23061.
30 D. W. Pierce and S. G. Boxer, *Biophys. J.*, 1995, **68**, 1583.
31 L. Wang, Q. Zhang, X. Wang, J. Liu and J. Yang, *J. Appl. Polym. Sci.*, 2011, **122**, 2552.
32 Q. Zhang, Y. Zhang, Q. Wei, X. Wang, J. Liu, J. Yang and C. Zhao, *J. Appl. Polym. Sci.*, 2011, **120**, 2648.
33 H. Wang, G. Jian, S. Yan, J. B. DeLisio, C. Huang and M. R. Zachariah, *ACS Appl. Mater. Interfaces*, 2013, **5**, 6797.
34 B. Almeria, W. W. Deng, T. M. Fahmy and A. Gomez, *J. Colloid Interface Sci.*, 2010, **343**, 125.
35 X. Y. Yang, A. Leonard, A. Lemaire, G. Tian and B. L. Su, *Chem. Commun.*, 2011, **47**, 2763.
36 T. Takami and Y. Murakami, *Langmuir*, 2014, **30**, 3329.
37 M. S. Nikolic and J. Djonlagic, *Polym. Degrad. Stab.*, 2001, **74**, 263.
38 A. Nelson, *Biophys. J.*, 1999, **76**, 1639.
39 G. Fabregat, G. Ballano, E. Armelin, L. J. del Valle, C. Cativiela and C. Alemán, *Polym. Chem.*, 2013, **4**, 1412.
40 G. C. Smith, *J. Electron Spectrosc. Relat. Phenom.*, 2005, **148**, 21.

41 E. Llorens, H. Ibañez, L. J. del Valle and J. Puiggalí, *Mater. Sci. Eng., C*, 2015, **49**, 472–484.
42 H. Y. Wang, J. H. Ji, W. Zhang, Y. H. Zhang, J. Jiang, Z. W. Wu, S. H. Pu and P. K. Chu, *Acta Biomater.*, 2009, **5**, 279.
43 J. F. Moulder, W. F. Stickle, P. E. Sobol and K. D. Bomben, *Handbook of X-ray Photoelectron Spectroscopy*, Perkin-Elmer Corp, Eden Prairie, MN, USA, 1992.
44 Z. Yang, S. Yuan, B. Liang, Y. Liu, C. Choong and S. O. Pehkonen, *Macromol. Biosci.*, 2014, **14**, 1299.
45 K. Chrissafis, K. M. Paraskevopoulos and D. N. Bikiaris, *Thermochim. Acta*, 2005, **435**, 142.
46 H. Zhao, Y.-Z. Wang, D. Y. Wang, B. Wu, D.-Q. Chen, X.-L. Wang and K.-K. Yang, *Polym. Degrad. Stab.*, 2003, **80**, 135.
47 Y. Wang, X. Yang, W. Liu, F. Zhang, Q. Cai and X. Deng, *J. Microencapsulation*, 2013, **30**, 490.
48 J. Xie, W. J. Ng, L. Y. Lee and C. H. Wang, *J. Colloid Interface Sci.*, 2008, **317**, 469.
49 Y. H. Lee, F. Mei, M. Bai, S. Zhao and D. R. Chao, *J. Controlled Release*, 2010, **145**, 58.
50 A. Bohr, J. Kristensen, M. Dyas, M. Edirisinghe and E. Stride, *J. R. Soc., Interface*, 2012, **9**, 2437.